



# Micro-Scale Pore-Throat Heterogeneity of Tight Oil Sandstone Reservoirs and Its Influence on Fluid Occurrence State

Qing Guo<sup>1,2\*</sup>, Mancang Dong<sup>3</sup>, Hengbo Mao<sup>4</sup> and Jiangtao Ju<sup>5</sup>

<sup>1</sup>Baile School of Petroleum Engineering, Lanzhou City University, Lanzhou, China, <sup>2</sup>State Key Laboratory of Continental Dynamics, Northwest University, Xi'an, China, <sup>3</sup>Fuxian Oil Production Plant, Yanchang Petroleum (Group). Ltd., Fuxian, China, <sup>4</sup>No.12 Oil Production Plant, Changqing Oilfield Company, PetroChina, Qingyang, China, <sup>5</sup>No.5 Oil Production Plant, Changqing Oilfield Company, PetroChina, Xi'an, China

## OPEN ACCESS

### Edited by:

Wenlong Ding,  
China University of Geosciences,  
China

### Reviewed by:

Xiaowei Lv,  
Chengdu University of Technology,  
China  
Ying Tang,  
Xi'an Shiyou University, China

### \*Correspondence:

Qing Guo  
qingguo133@126.com

### Specialty section:

This article was submitted to  
Structural Geology and Tectonics,  
a section of the journal  
Frontiers in Earth Science

**Received:** 02 June 2022

**Accepted:** 15 June 2022

**Published:** 08 August 2022

### Citation:

Guo Q, Dong M, Mao H and Ju J  
(2022) Micro-Scale Pore-Throat  
Heterogeneity of Tight Oil Sandstone  
Reservoirs and Its Influence on Fluid  
Occurrence State.  
Front. Earth Sci. 10:959796.  
doi: 10.3389/feart.2022.959796

Quantitatively characterizing the micro-scale heterogeneity of pore throats in tight sandstone reservoirs is the key to accurately describing the influence of pore structures on fluid occurrence characteristics. In this study, taking the Chang 6 Member of the Yanchang Formation in the Huaqing area of the Ordos Basin as an example, the pore-throat heterogeneity of tight sandstone reservoirs and its influence on the fluid occurrence state have been systematically studied using cast thin section, scanning electron microscope, X-ray diffraction, constant velocity mercury intrusion, and nuclear magnetic resonance tests. The main types of pores developed in the target layer were intergranular pores, followed by feldspar dissolution pores. The radius distribution of the intergranular pores is between 5.0 and 210  $\mu\text{m}$ , with an average value of 50.27  $\mu\text{m}$ . In addition, the pore combination types with the best petrophysical properties are the intergranular pore type, the intergranular-dissolution pore type, and the dissolution-intergranular pore type; the average permeability and porosity are 0.62 mD, 0.40 mD, 0.44 mD, and 12.0, 12.3, 12.3%, respectively. The target sandstones contain four typical  $T_2$  relaxation time types. The large-pore-fine-throat combination reservoir has the best petrophysical properties. The larger the pore-throat uniformity value, the more uniform the pore-throat radius, and the greater the reservoir permeability. Therefore, the uniformity of throat development controls the seepage capacity of the tight reservoirs. The movable fluid saturation of different pore types has obvious differences. The movable fluid saturations at the 0.1 and 0.5  $\mu\text{m}$  pore diameters of the macro-pore-fine-throat and macro-pore-micro-throat reservoirs both show an obvious inflection point, and the movable water saturation is higher with a larger throat radius.

**Keywords:** pore-throat heterogeneity, tight oil sandstone, fluid occurrence state, physical properties, permeability

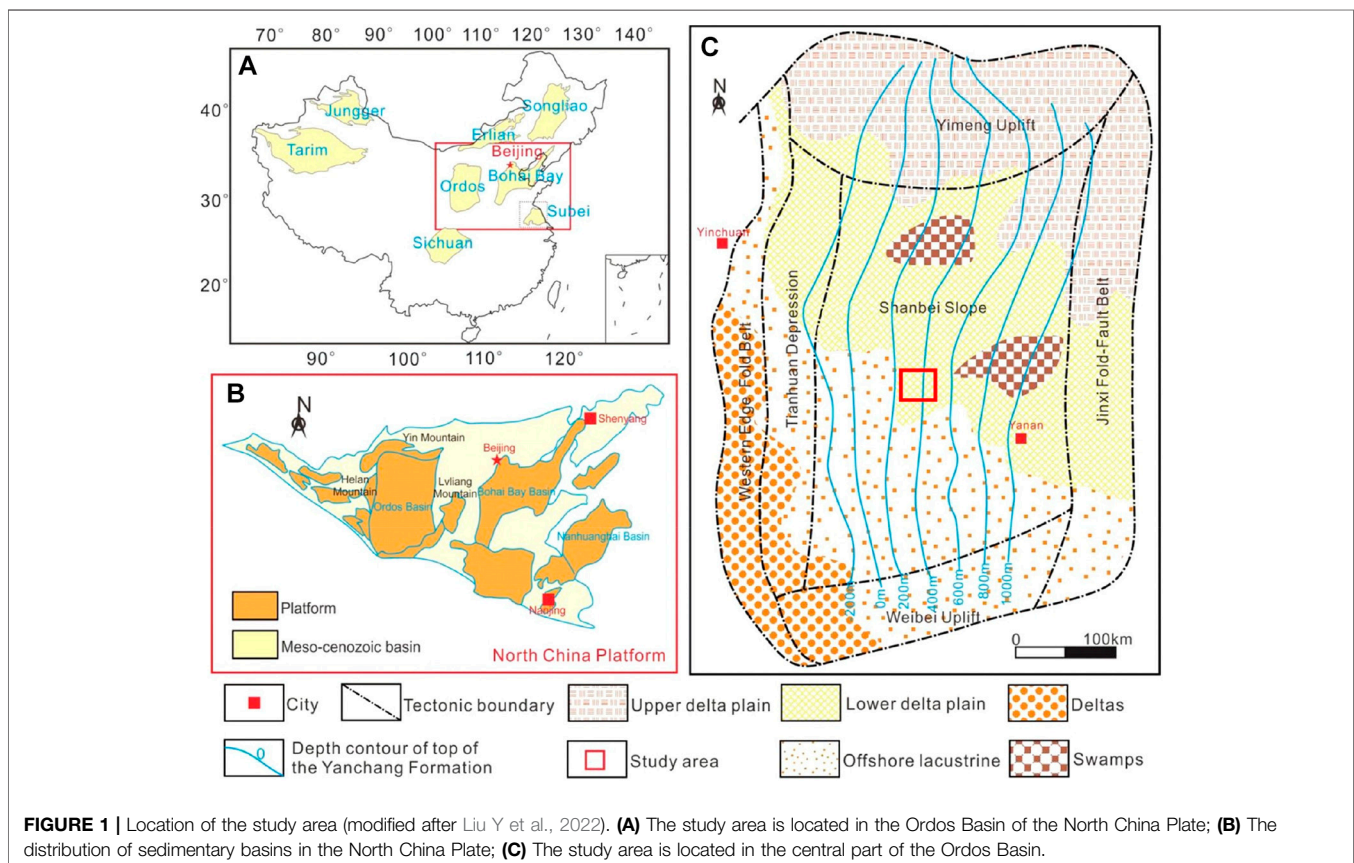
## 1 INTRODUCTION

Tight oil reservoirs refer to oil layers such as sandstones and carbonate rocks with an overburden matrix permeability less than 0.2 mD or an air permeability less than 2 mD (Zou et al., 2012; Anovitz et al., 2013; Anovitz and Cole., 2015; Lai et al., 2018a; Cao et al., 2020). Tight sandstone reservoirs have the characteristics of small pore-throat size, strong heterogeneity, and complex pore structures (Lai and Wang., 2015; Cai, 2020; Hong et al., 2020; Bukar et al., 2021). The occurrence states and the final recoverability of oil and gas in tight reservoirs are the most concerning issues in the exploration and production of oil and gas (Gier et al., 2008; Desbois et al., 2011; Chen et al., 2014; Ghanizadeh et al., 2015; Lai et al., 2018b).

Reservoir heterogeneity is the inhomogeneous changes of the internal properties of reservoirs caused by the influence of depositional environment, diagenesis, and tectonic action during the deposition and burial processes (Kwak et al., 2017; Meng et al., 2017; Li et al., 2019; Hower and Groppo., 2021; Huang et al., 2021). Obviously, the sorting coefficients of pores and throats cannot accurately reflect the heterogeneity of the microscopic pore structures of tight sandstone reservoirs. In fact, in the reservoir storage of tight sandstone reservoirs, there are certain differences in the distribution of pore throats in different pore-throat intervals (Ma, 2005; Jiang et al., 2017; Pang et al., 2019; Liu

et al., 2020; Kang, 2021). Therefore, quantitatively characterizing the micro-scale heterogeneity of pore-throats in tight sandstone reservoirs is the key to accurately describing the influence of pore structures on fluid occurrence characteristics (Lei et al., 2012; Sun et al., 2014; Li et al., 2019; Luo et al., 2019; Ren et al., 2019; Liu J et al., 2022). Pore-throat heterogeneity has a significant effect on tight reservoir permeability. The configuration of pores and throats determines the path of fluid flow and the resistance they need to overcome, which ultimately affects fluid flowability or reservoir permeability. Permeability is a core factor in determining reservoir productivity (Sun et al., 2014; Luo et al., 2019; Ren et al., 2019).

At present, the main problem in the efficient development of the Chang 6 Member of Yanchang Formation in the Ordos Basin is that the influence mechanism of microscopic pore structures on oil productivity is not clear. In this study, taking the Chang 6 Member of the Yanchang Formation in the Huaqing area of the Ordos Basin as an example, the pore-throat heterogeneity of tight sandstone reservoirs and its influence on the fluid occurrence state have been systematically studied using cast thin section, scanning electron microscope, X-ray diffraction, constant velocity mercury intrusion, and nuclear magnetic resonance tests. This study can provide scientific guidance for the scientific formulation of tight oil reservoir recovery programs.



## 2 MATERIALS AND METHODS

### 2.1 Study Area

The study area is located in the Huaqing area of the Ordos Basin (Figure 1). The area is adjacent to the Changguan Temple in the north, the Resettlement Farm in the south, Yuancheng city in the west and Majiabian city in the east, with an area of about 6,150 km<sup>2</sup>. Its tectonic location is located in the southern part of the Yishan Slope. The target layer is the Chang 6 Member of the Upper Triassic Yanchang Formation, and it belongs to the delta front facies deposits.

### 2.2 Constant-Rate Mercury Intrusion Technology

Constant-rate mercury intrusion technology can provide detailed information on pore structures by monitoring the pressure fluctuations during mercury injection. Constant-rate mercury intrusion can measure the number of throats during the experiments; it has overcome the shortcomings of conventional mercury intrusion. In this study, the mercury was injected into the core at a low injection rate (0.00005 ml/min). During the mercury injection process, the pressure drops and rises periodically, and the experiment ends when the pressure reaches 900 psi (6.2055 MPa).

An ASPE-730 constant-speed mercury intrusion device was used to conduct the constant-speed mercury intrusion experiments. The specific steps taken in the experiments are as follows:

- (1) First, drilling a standard core with a diameter of 2.5 cm from a full-diameter core, then drying it at an experimental temperature of 23°C.
- (2) Then, measuring the porosity of the standard core after drying via the gas measurement method.
- (3) Using the gas measurement method to measure the permeability of the standard core after drying.
- (4) Selecting representative standard cores for constant-rate mercury intrusion experiments.
- (5) Evacuating the rock samples and immersing them in the mercury solution.
- (6) Adjusting the experimental temperature to 25°C, the humidity to 65–75%, and the mercury injection rate to 0.000001 ml/s~1 ml/min. The contact angle was 140° and the surface tension was 485 dyne/cm. Real-time monitoring and automated data acquisition were output through computer systems.

### 2.3 Nuclear Magnetic Resonance Technology

The interior of the reservoir is saturated with three-phase fluids of oil, gas, and water. The occurrence states of these fluids in the reservoir can be divided into two categories: one is bound fluid state; the other is free fluid state. When the fluid-contained rock sample is in a static magnetic field, the hydrogen nuclei contained in the fluid are easily polarized by the magnetic field. NMR

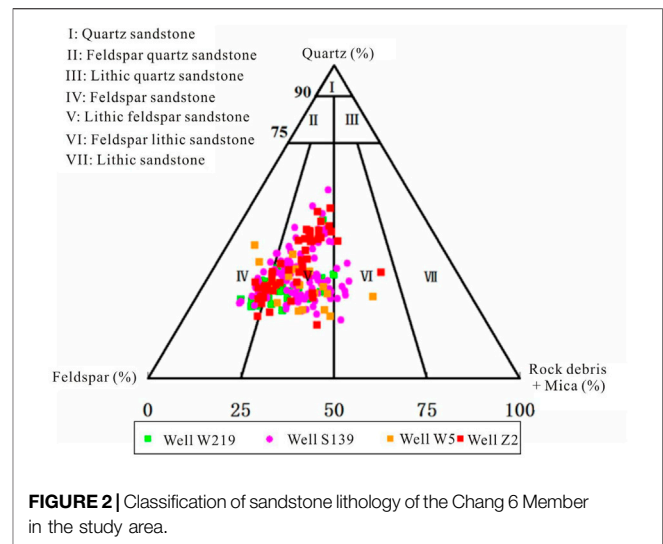


**FIGURE 2** | Classification of sandstone lithology of the Chang 6 Member in the study area.

technology uses the inverse relationship between the hydrogen nuclear relaxation rate and the pore size of the reservoir rock to study the pore structures of rocks, and to determine the movable fluid saturation and the occurrence states of fluids of the reservoir. When the pore radius of the rock is too small, the fluid in it cannot flow due to the large capillary force and the specific surface binding effect. NMR experiments were used to determine the occurrence characteristics of movable fluids and the distribution of pore throats based on the  $T_2$  spectral relaxation time and different spectral peak characteristics. The calculation relationship between the movable fluid porosity ( $\Phi_m$ , %), the movable fluid saturation ( $S_m$ , %), and the water-measured porosity ( $\Phi$ , %) is:  $\Phi_m = S_m \times \Phi / 100$ .

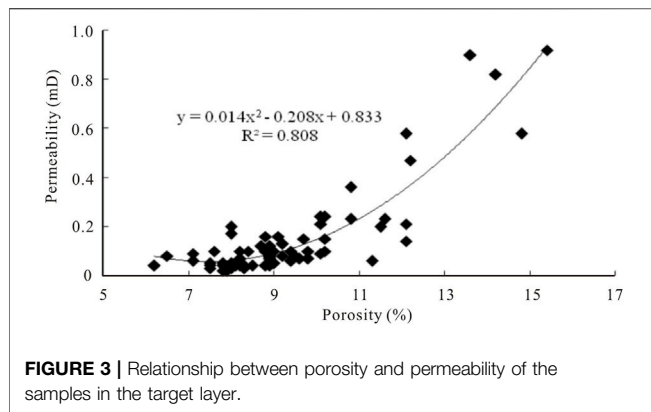
A Magnet 2000 instrument was used to perform NMR  $T_2$  measurements at a constant temperature of 20°C. The specific experimental steps are as follows:

- (1) Selecting a representative standard core with a diameter of 2.5 cm.
- (2) Drying the standard core.
- (3) Measuring the porosity and air permeability of the samples.
- (4) Saturating the samples with the simulated formation water (total salinity is 25,000 mg/L).
- (5) Calculating the porosity of cores using the difference between the wet weight and the dry weight.
- (6) Performing nuclear magnetic resonance  $T_2$  measurements on the standard core saturated with simulated formation water.

## 3 RESULTS

### 3.1 Rock Type and Mineral Composition

According to the observation results of cast thin sections, the sandstones of the Chang 6 oil layer group in this area have the characteristics of “low quartz and high feldspar content.” The main lithologies of the Chang 6 Member include feldspar sandstone and lithic feldspar sandstone. The quartz content



ranges from 28 to 30%, the feldspar content ranges from 34 to 40%, and the debris content ranges from 10 to 12% (**Figure 2**). The debris components are mainly composed of metamorphic rocks with a content of 5.5–7.5%, followed by the sedimentary rocks, with a content of 2.5–3.2%, and the igneous rocks, with a relatively small content of 1.2–2.5%. In addition, there are detrital minerals such as mica and chlorite.

According to the results of the cast thin sections of the rock samples, the maximum particle size distribution of the Chang 6 reservoir sandstone in the study area is 0.10–0.90 mm, and the main particle size is 0.01–0.50 mm. The cements of the Chang 6 sandstone mainly include hydromica, chlorite, iron calcite, iron dolomite, calcite, and siliceous components.

### 3.2 Reservoir Petrophysical Properties

The porosity of the Chang 6 reservoir in the study area is between 8 and 20.9%, the main interval is between 8 and 12%, and the average porosity is 11.6%; the permeability is between 0.08 and 17.49 mD, the main interval is between 0.1 and 0.5 mD, and the average permeability is 0.355 mD. Therefore, the Chang 6 Member belongs to the low-porosity-ultra-low-porosity, low-permeability-ultra-low permeability reservoir.

It can be seen from **Figure 3** that the correlation between the porosity and permeability of the samples satisfies the quadratic polynomial relationship, and the correlation coefficient is 0.808.

### 3.3 Pore Type

The main types of pores developed in the Chang 6 reservoir in the study area are intergranular pores, intergranular dissolution pores, feldspar dissolution pores, debris dissolution pores, and intercrystalline pores, among which intergranular pores and feldspar dissolution pores are the main ones.

Residual intergranular pores refer to the remaining part of the initial intergranular pores during deposition and filled with cements (**Figures 4A,B**). These pores are further subdivided into compacted intergranular pores, interstitial intergranular pores, and dissolution intergranular pores according to the degree of filling, dissolution, and compaction. The shapes of these pores are mostly polygonal, triangular, and irregular (Li and Zhang, 2011; Li et al., 2017). The samples mainly developed cement-type and dissolution-type intergranular pores. These pores generally exist between framework minerals, and the

surface of the pores are often coated with chlorite, while secondary quartz is occasionally to be seen; the other kind of pores exists between the framework minerals and clay minerals, which are the products of clay minerals under compression and bending, and the pores are mostly triangular or meniscus. The absolute content of the intergranular pores is between 0.2 and 12.0%, with an average value of 3.81% and a relative average content of 71.06%. Statistics show that the radii of different types of pores vary greatly, and the pore radii of the target layer are mainly between 5.0 and 210  $\mu\text{m}$ , with an average value of 50.27  $\mu\text{m}$ . Intergranular pores are the main oil and gas storage space in the target layer.

The dissolution pores developed in the target layer are mainly feldspar dissolution pores, followed by the debris dissolution pores and the cement dissolution pores. Feldspar dissolution pores are the most important type of dissolution pores. It undergoes selective grain boundary and intragranular dissolution along the soluble part and cleavage of feldspar grains, and presents various pore morphologies, such as cleavage dissolution, mold dissolution, and irregular grain boundary dissolution (**Figures 4C,D**). The dissolution pores and intergranular pores of feldspar particles can be connected together to form super-large pores, and the pore sizes vary widely (15–200  $\mu\text{m}$ ). The absolute content of feldspar dissolution pores is between 0.1 and 2.0%, with an average content of 0.65%.

Intercrystalline micro-pores are also an important type of pore, which includes primary and secondary cement intercrystalline micro-pores (Luo et al., 2018; Mirzaei-Paيمان and Ghanbarian, 2021). It can be seen that the radius of such pores is generally less than 5  $\mu\text{m}$  under the scanning electron microscope (**Figures 4E,F**). The primary intercrystalline micro-pores in the samples are mainly cleavage intercrystalline micro-pores of mica. The intercrystalline pores of framework minerals are generally formed by the dissolution of feldspar minerals. The intercrystalline micro-pores mainly include authigenic chlorite, illite, and micro-pores between secondary quartz. Statistics show that the absolute content of the intergranular micro-pores is between 0.01 and 0.6%, with an average value of 0.12%.

The final statistical results show that the pore combination types with the best petrophysical properties are the intergranular pore type, the intergranular-dissolution pore type, and the dissolution-intergranular pore type; their average permeability and porosity are 0.62 mD, 0.40 mD, 0.44 mD, and 12.0, 12.3, 12.3%, respectively. The micro-pore type has a small average pore size, low surface porosity, and the lowest seepage capacity.

### 3.4 Occurrence Characteristics of Movable Fluids

In this experiment, 13.895 ms was taken as the limit value of  $T_2$  relaxation time of movable and bound fluids. Movable fluid saturation is the percentage of the amplitude of each point, with  $T_2$  relaxation time greater than 13.895 ms on the  $T_2$  spectrum. Conversely, the bound fluid saturation is the percentage of the amplitudes of the points where the  $T_2$  relaxation time is less than 13.895 ms on the  $T_2$  spectrum.

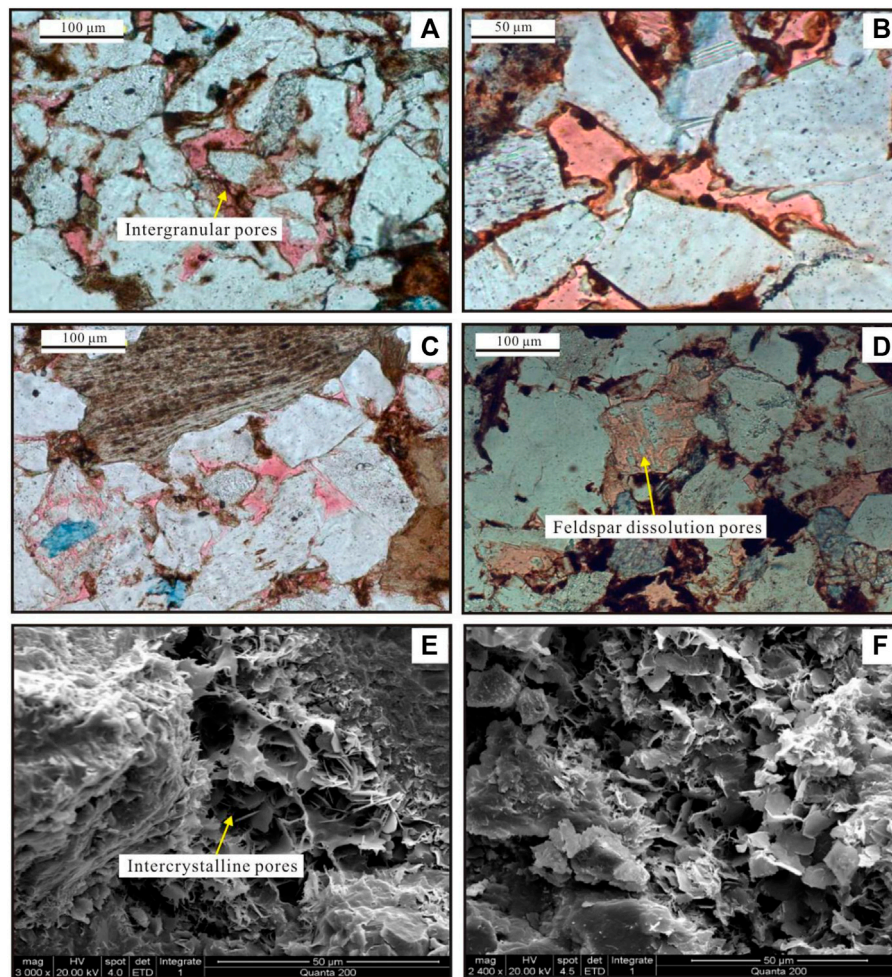


**FIGURE 4** | Development characteristics of different types of pores in the target layer. **(A)** Intergranular pores, Well H259, 2,191.00 m; **(B)** Intergranular pores, Well H470, 2,140.8 m; **(C)** Feldspar dissolution pores, Well H408, 1,960.95 m; **(D)** Feldspar dissolution pores, Well H284, 2,181.95 m; **(E)** Illite and chlorite intercrystalline pores, Well H156, 2,084.28 m; **(F)** Illite and chlorite intercrystalline pores, Well H72, 2,069.00 m.

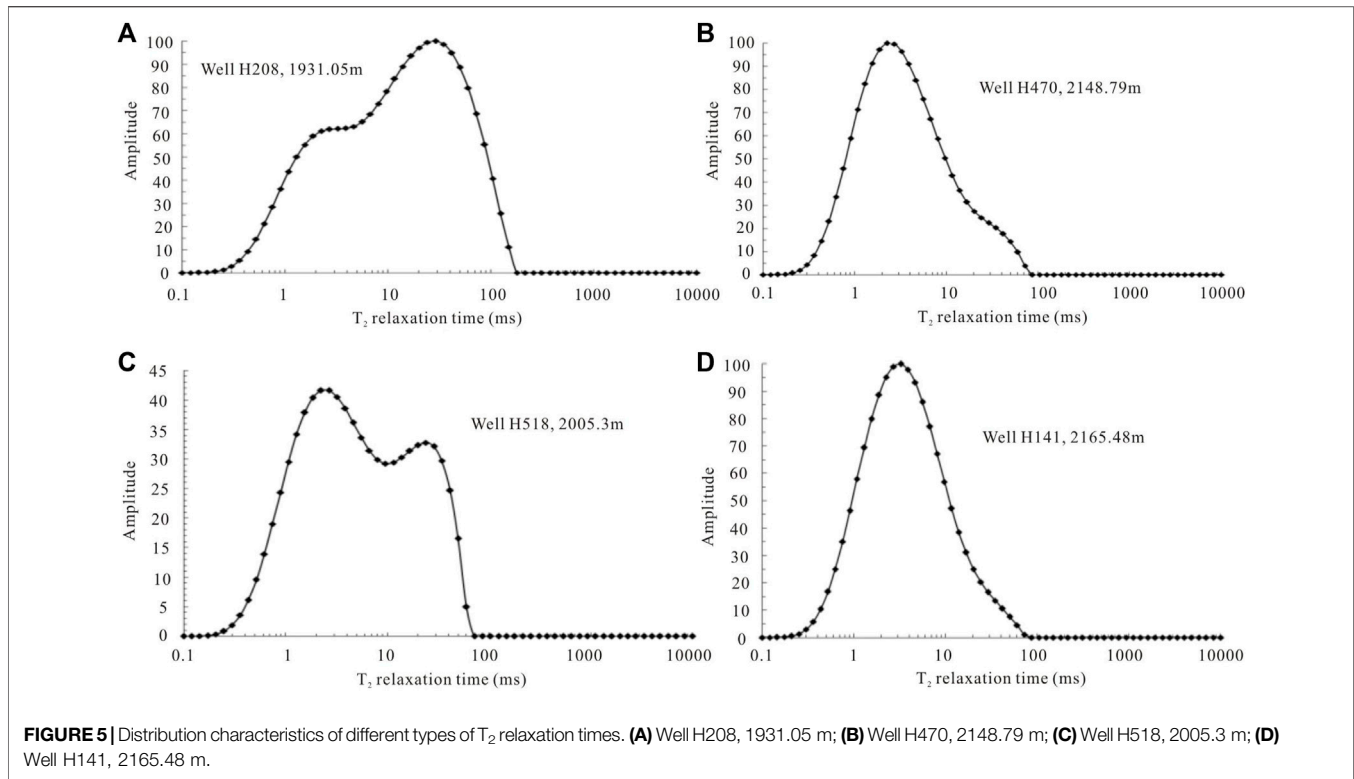
In order to achieve the comparative analysis of samples with different pore-throat matching relationships and different permeability levels, the screening of experimental samples has comprehensively considered the results of casting thin sections, scanning electron microscopy, and petrophysical property tests. On the basis of fully considering the characteristics of sedimentation and diagenesis, four groups of samples with different permeability levels were selected, respectively. Furthermore, in each group, one sample was selected for comparison of the microscopic pore structures.

The target sandstones contain four typical  $T_2$  spectral relaxation time types (**Figure 5**):

(1) Bimodal type (the left peak is lower than right peak). For the first type, the H208 rock sample in **Figure 5A** is taken as an example, and its  $T_2$  spectral distribution is bimodal type. The areas on both sides of the 13.895 ms time limit are basically equal, the movable fluid saturation is 45.55%, and the irreducible water saturation is 54.45%. It shows that the

movable fluid saturation is slightly larger than the irreducible water saturation.

- (2) Asymmetric unimodal type. The  $T_2$  spectrum distribution of the H470 rock sample showed an asymmetric single peak type (**Figure 5B**). Its single peak is almost on the left side of the time limit of 13.895 ms, the movable fluid saturation is 11.37%, and the irreducible water saturation is 88.63%. This means that there are few movable fluids and a lot of bound water inside the rock;
- (3) Bimodal type (the left peak higher than right peak). The  $T_2$  spectrum distribution of the H518 rock sample is bimodal (**Figure 5C**). The area on the left side of the time limit of 13.895 ms is much larger than the area on the right side. The movable fluid saturation is 29.04%, and the irreducible water saturation is 70.96%. This means that the movable fluid saturation is less than the irreducible water saturation;
- (4) Narrow single peak type. The  $T_2$  spectrum of the H141 rock sample is a narrow single peak type (**Figure 5D**). The single-peak body is to the left of the 13.895 ms time limit. The



movable fluid saturation is 9.09%, and the irreducible water saturation is 90.91%.

This study shows that the  $T_2$  spectral cutoff value of the low-permeability movable fluid is low, that the movable fluid saturation in the pores is low, and that the movable fluid saturation value and the movable fluid porosity value fluctuate greatly.

## 4 DISCUSSION

### 4.1 Correlation Between Pore Structure Parameters and Petrophysical Property Parameters

The pore-throat characteristic parameters of the capillary pressure curves of 28 samples were statistically analyzed, and the correlations between each pore-throat characteristic parameter and reservoir porosity and permeability were analyzed. The results show that the permeability has a good correlation with the displacement pressure and the maximum pore-throat radius, and the correlation coefficients are both 0.56 (**Figures 6A,B**). Moreover, the correlation between the porosity and the maximum mercury inflow saturation is also good, and it has a correlation coefficient of 0.51 (**Figure 6C**). However, the petrophysical parameters have poor or no correlation with other pore-throat characteristic parameters.

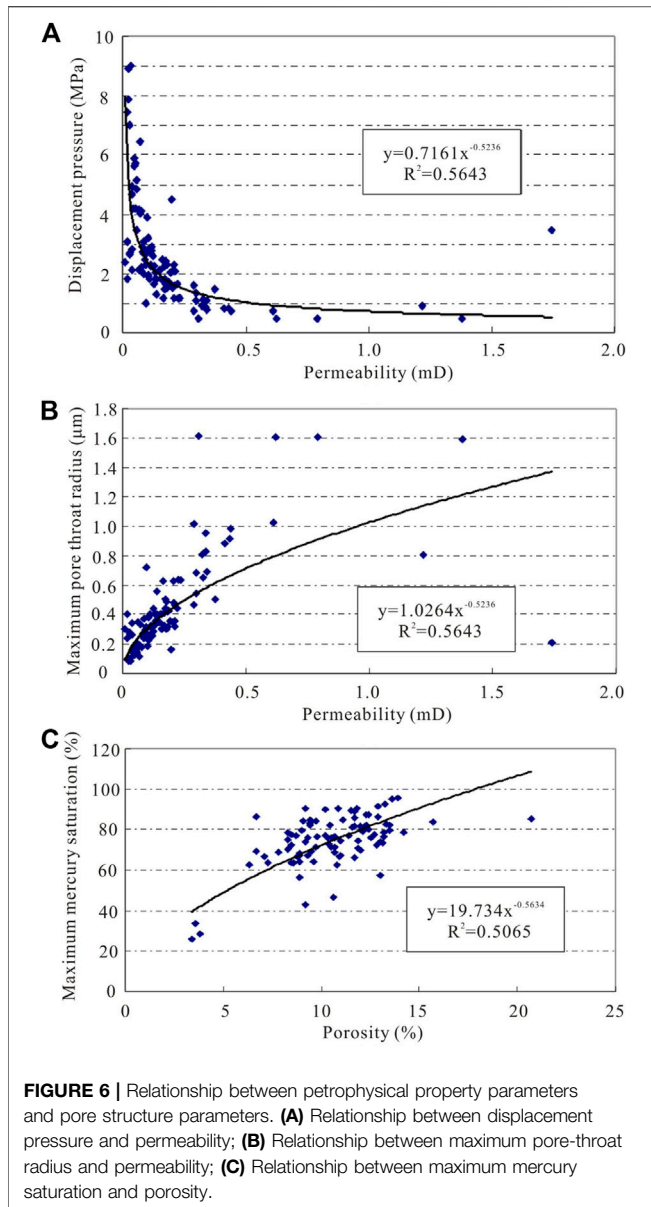
### 4.2 Influence of Pore-Throat Heterogeneity on Reservoir Physical Parameters and Permeability Contribution

Reservoir heterogeneity is the inhomogeneous change of internal properties caused by the influence of depositional environment, diagenesis, and tectonic action (Sebacher et al., 2017; Wang A. et al., 2018; Malatesta et al., 2018; Lan et al., 2021; Yang et al., 2021). Under the guidance of information entropy theory, this study takes different types of pore-throat assemblages and classifications as the starting point to construct a quantitative characterization model of pore-throat micro-scale heterogeneity in tight oil reservoirs.

- (1) First, under the guidance of the information entropy theory, the information entropy of different pore and throat distributions is calculated using the MATLAB programming language:

$$H = -\sum_{i=1}^m z_i \ln z_i \quad (1)$$

where  $z_i$  is the percentage of the  $i$ th pore radius and throat radius, which is obtained from the frequency spectrum of the pore radius and throat radius distribution. When the travel frequency of different pores and throat sizes is the same, i.e. when  $z_1 = \dots = z_n = 1/N$ , the entropy value reaches the maximum value of  $\ln N$ , indicating that the size distribution of pores and throats has reached a uniform state.



In the same way, the information entropy can be used to analyze the relative uniformity of the size distribution of pore radii and throat radii within the interval of different pore radii and throat radii.

- (2) In practical applications, there are differences in the size distribution characteristics of pores and throats of different types of pore-throat combination reservoirs (Meng et al., 2017; Huang et al., 2021). Therefore, the uniformity  $M$  (the ratio of the actual entropy value to the maximum entropy value) of the size distribution of pore radius and throat radius is introduced to characterize the uniformity of the size distribution of pores and throats in different types of pore-throat combination reservoirs, namely:

$$M = \frac{-\sum_{i=1}^n (z_i \ln z_i)}{\ln N} \quad (2)$$

The greater the uniformity, the more uniform the distribution of the parameter.

- (3) In order to use the information entropy to determine the weight of pores and throats, and to solve the joint uniformity of pores and throats, the degree of dispersion of pores and throats is calculated first (Sebacher et al., 2017; Malatesta et al., 2018). Generally, the degree of dispersion of the  $j$ th index (pores, throats) depends on  $M_j$ :

$$h_j = 1 - M_j \quad (3)$$

The more dispersed the value of the  $j$ th index (pores, throats), the higher the importance of the  $j$ th index (pores, throats). Among all  $n$  indexes (pores, throats), the weight of the  $j$ th index (pores, throats) can be determined using Eq. 4.

$$w_j = \frac{h_j}{\sum_{i=1}^n h_j} \quad (4)$$

where  $j=1,2$ .

$$I = W_1 M_1 + W_2 M_2 \quad (5)$$

- (4) Combining the uniformity information entropy of pores and throats, the generated joint uniformity information entropy  $I$  is:

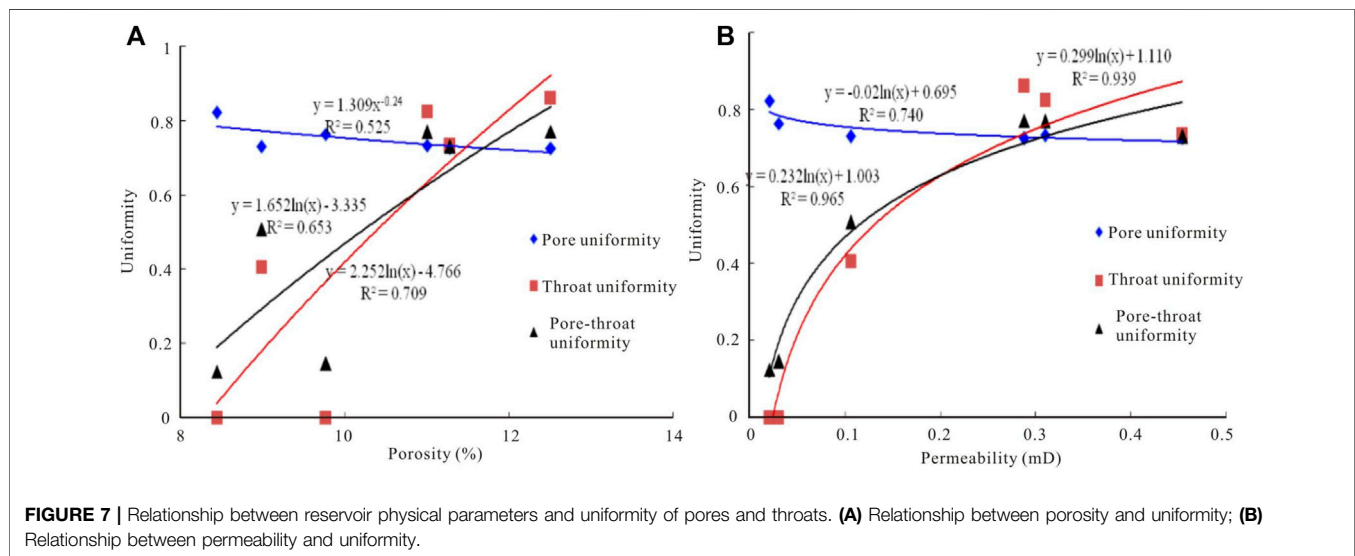
Based on steps (3) and (4), combined with steps (1) and (2), the uniformity of pore radius and throat radius of six rock samples from the Chang 6 reservoir in the study area is obtained. The results are shown in Table 1.

It can be seen from Table 1 that, for the reservoirs with macro-pore-micro-throat combination (rock samples H269, H470, and H141), the information entropy of the combined pore-throat uniformity ranges from 0.1240 to 0.0.5078, with an average value of 0.2593. For reservoirs with macro-pore-micro-throat combination (rock samples H518 and H259), the information entropy of the combined pore-throat uniformity ranges from 0.7301 to 0.0.7708, with an average value of 0.0.7504. The information entropy of the pore-throat uniformity of the H208 rock sample is 0.7693. The above results show that the pore-throat distribution of the reservoir with the macro-pore-fine-throat combination is the best, followed by the macro-pore-micro-throat combination, and the reservoir with the macro-pore-micro-throat combination has the worst pore-throat uniformity. This shows that the microscopic heterogeneity of the Chang 6 reservoir in the study area is mainly controlled by the uniformity of throat distribution.

The study found that the smaller the permeability of the sample, the more concentrated the distribution of the contribution of the throat to the rock permeability, and the larger the contribution peaks. With the gradual increase of rock permeability, the distribution interval of throats becomes

**TABLE 1** | Pore-throat uniformity of reservoirs with different types of pore-throat combinations.

Number	Depth (m)	Porosity (%)	Permeability (mD)	Pore Uniformity	Throat Uniformity	Pore-throat Uniformity
H259	2,187.30	12.51	0.288	0.7249	0.8629	0.7708
H269	1,943.90	8.44	0.021	0.8224	0	0.1241
H470	2,148.79	9.77	0.031	0.7639	0	0.1460
H518	2,005.56	11.28	0.454	0.7269	0.7332	0.7301
H141	2,165.48	8.98	0.106	0.7304	0.4067	0.5078
H208	1,931.05	11.00	0.310	0.7324	0.8260	0.7693
H169	2,109.75	10.92	0.345	0.7295	0.7631	0.7409
H489	2,017.93	9.11	0.238	0.7345	0.6235	0.6792
H307	2,201.20	8.63	0.207	0.7296	0.5960	0.6537



wider, the number of large throats increases, and the contribution of small throats to permeability decreases significantly. Then, the contribution of the large throats to the rock permeability increases, and the throat radius corresponds to the contribution peaks moves to the side of large throats. For example, the throat radii corresponding to the contribution peaks of the two samples of H208 and H518 are 1.1 and 0.6  $\mu\text{m}$ , respectively. At this time, the number of large throats that mainly contribute to the rock permeability increases, and the peak value of the contribution decreases significantly. The fundamental reason for the poor petrophysical properties (especially permeability) of the low-permeability tight sandstones lies in the large proportion of small throats.

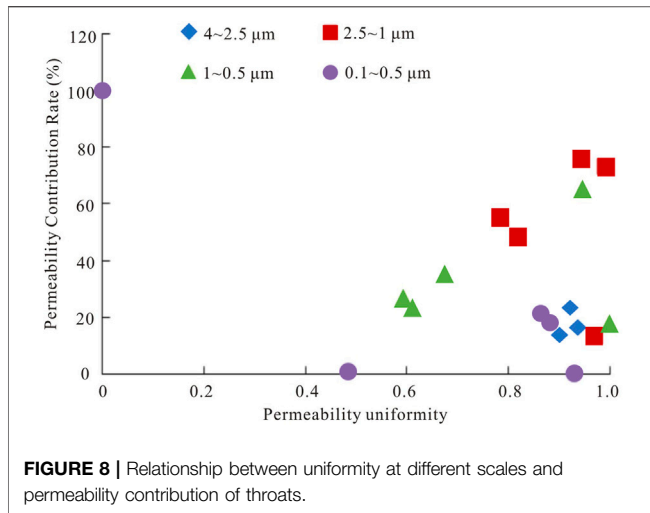
Statistics show that the H208 sample with a large-pore-fine-throat reservoir (permeability  $>0.3$  mD, low permeability) has a peak throat radius of 1.1  $\mu\text{m}$ , and the cumulative contribution to the rock permeability is 60.19%. For the H259 sample with macro-pore-micro-throat (permeability of  $0.3$  mD  $< K < 0.1$  mD, ultra-low permeability), the cumulative contribution of the permeability corresponding to the peak throat radius of 0.4  $\mu\text{m}$  is 87.6%. In addition, the cumulative contribution of the permeability corresponding to the peak throat radius of 0.2  $\mu\text{m}$  for the H141 sample with macro-pore-micro-throat

(permeability  $K < 0.1$  mD) is 96.39%, and the main peak is in the micro-throat grade range.

It can be seen from **Figure 7** that the relationship between the permeability and uniformity of pore-throats is better than that of porosity. This is because permeability is the most direct factor determining the pore structures of tight reservoirs, while porosity is an indirect factor.

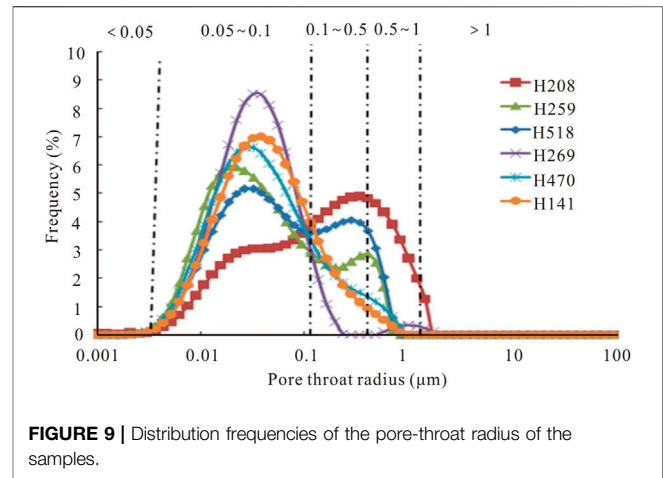
The pore uniformity is negatively correlated with the porosity, and the correlation coefficient  $R^2$  is 0.525. This shows that the larger the value of the pore uniformity, the more uniform the development degree of pores, but the reservoir porosity will decrease; the throat uniformity is positively correlated with porosity, and the correlation coefficient  $R^2$  is 0.653, indicating that the larger the throat uniformity value, the more uniform the development degree of throats, and the greater the reservoir porosity; in addition, the pore-throat uniformity is positively correlated with porosity, and the correlation coefficient  $R^2$  is 0.709, indicating that the larger the pore-throat uniformity value, the more uniform the pore-throat boundary, and the greater the reservoir porosity (Rezaee et al., 2012; Mahmud et al., 2020; Mohammed et al., 2021).

The comparative results show that the uniformity of the throat development controls the effectiveness of the reservoir space



(Shanley and Cluff, 2015; Xi et al., 2016; Qiao et al., 2020; Qie et al., 2021). The pore uniformity is negatively correlated with permeability, and the correlation coefficient  $R^2$  is 0.749, indicating that the larger the pore uniformity value, the more uniform the pores, but the reservoir permeability will decrease; the throat uniformity is positively correlated with porosity, and the correlation coefficient  $R^2$  is 0.939, indicating that the larger the throat uniformity value, the more uniform the throats, and the greater the reservoir permeability; the pore-throat uniformity is positively correlated with rock permeability, and the correlation coefficient  $R^2$  is 0.978, indicating that the larger the pore-throat uniformity value, the more uniform the pore-throat radius, and the greater the reservoir permeability. Therefore, the uniformity of throat development controls the seepage capacity of the reservoir (Zhao et al., 2015; Saein and Riahi, 2017; Yin et al., 2018; Santosh and Feng, 2020; Zhang et al., 2020).

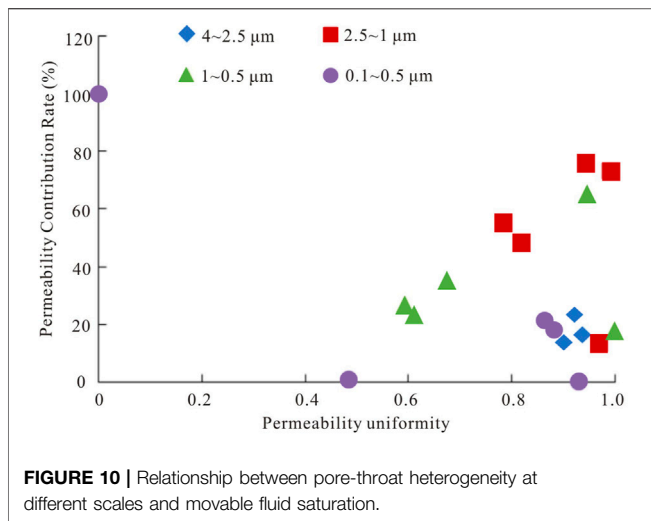
It can be seen from **Figure 8** that the throat radius between 2.5 and 4.0  $\mu\text{m}$  is only developed in the macro-pore-micro-throat combination type reservoir (H518 rock sample), but the contribution to permeability is relatively small (only 16.61%). This shows that the throats of 2.5–4.0  $\mu\text{m}$  are less developed in this type of reservoir, thus it has little effect on the seepage capacity of the reservoir. When the throat radius is between 1.0 and 2.5  $\mu\text{m}$ , the reservoirs of the large-pore-fine-throat (H208 rock sample) and the large-pore-micro-throat combination (H259, H518 rock samples) are uniformly developed. However, the reservoirs with macro-pore-micro-throat combination do not develop such kind of throats. The distribution of the uniformity (0.9917) and the permeability contribution (73.26%) of the throats of the large-pore-fine throat (rock sample H208) in this interval are better than those of the large-pore-micro-throat combination (rock samples H259 and H518). This shows that the throats of the 1.0–2.5  $\mu\text{m}$  interval control the seepage capacity of the large-pore-fine-throat combination reservoirs. However, its effect on the seepage capacity of the reservoir with large pores and fine throats (the average permeability contribution is 34.02%) is relatively small. When the throat radius is between 0.5 and 1.0  $\mu\text{m}$ , the reservoirs of the large-pore-fine-throat (H208 rock sample) and the large-pore-micro-throat combination (H259,



H518 rock samples) are uniformly developed. However, reservoirs with macro-pore-micro-throat combination do not develop such kind of throats. The average value of throat uniformity (0.9718) and the average value of permeability contribution (41.455%) in the large-pore-micro-throat combination (rock samples H259 and H518) in this interval are better than those of the macro-pore-fine-throat (H208 rock sample). This shows that the throat radius of 0.5–1.0  $\mu\text{m}$  can control the seepage capacity of the reservoir with the macro-pore-micro-throat combination better than the reservoir of the macro-pore-fine-throat combination (the uniformity of throat is 0.5931, and the permeability contribution is 26.73%). When the throat radius is between 0.1 and 0.5  $\mu\text{m}$ , all kinds of reservoirs develop such throats. Among them, the throat uniformity (0.9308) of the large pores and fine throats (H208 rock sample) in this interval is better than that of other reservoirs. However, in terms of contribution to the seepage capacity of the reservoir, this type of throat is the most developed in the macro-pore-micro-throat reservoir, and the permeability contribution value (100%) is the largest. The second is the reservoir with macro-pore-micro-throat combination (the average permeability contribution is 11.13%). However, in the reservoir with large-pore-fine-throat combination, this type of throat contributes the least to the seepage capacity of the reservoir (the contribution value of permeability is 0.001%).

### 4.3 Influence of Pore-Throat Heterogeneity on Fluid Occurrence

Statistical results show that, when the throat radius is greater than 0.1  $\mu\text{m}$ , the corresponding movable fluid percentages in the macro-pore-fine-throat, macro-pore-micro-/fine-throat, and macro-pore-micro-throat reservoirs are 45.55%, 24.45%, and 7.54%, respectively. When the throat radius is in the range of 0.1–0.5  $\mu\text{m}$ , the corresponding movable fluid saturations of the macro-pore-fine-throat, macro-pore-micro-/fine-throat, and macro-pore-micro-throat reservoirs are 34.19, 24.11%, and 7.02%, respectively. When the throat radius is in the range of 0.5–1.0  $\mu\text{m}$ , the corresponding movable fluid saturations of the macro-pore-fine-throat, macro-pore-micro-/fine-throat, and macro-pore-micro-throat reservoirs are 8.24, 0.34, and 0.43%, respectively. When the throat radius is



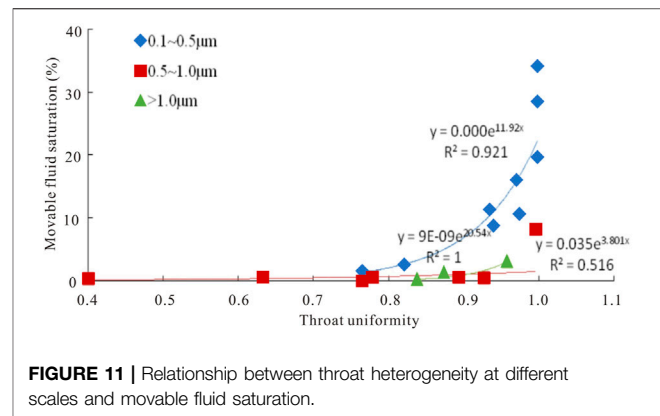
greater than 1.0  $\mu\text{m}$ , the corresponding movable fluid saturations of the macro-pore-fine-throat, macro-pore-micro-/fine-throat, and macro-pore-micro-throat reservoirs are 3.12%, 0, and 0.09%, respectively.

The movable fluids of different pore types have obvious differences (Wang L. et al., 2018; Shi et al., 2019; Yin and Wu, 2020; Zhou et al., 2021). Among them, the macro-pore-fine-throat reservoirs have the highest movable fluid saturation, followed by the macro-pore-micro-/fine-throat reservoirs, while the macro-pore-micro-throat reservoirs have the lowest movable fluid saturation. The macro-pore-fine-throat and macro-pore-micro-/fine-throat types show obvious inflection points at 0.1 and 0.5  $\mu\text{m}$ , and the larger the throat radius, the higher the movable water saturation (Figure 9).

It can also be seen from Figure 8 that the crude oil in the pore throat corresponding to the pore-throat radius  $>1.0 \mu\text{m}$  is preferentially produced and the remaining oil is less. However, most of the crude oil in the pore throats within the pore-throat radius of 0.1–1.0  $\mu\text{m}$  is recovered. The distribution of the residual fluid is closely related to its existing pore structures (Zhang et al., 2019; Yoshida and Santosh., 2020; Wang et al., 2021; Xue et al., 2021). The distribution of the  $T_2$  spectrum is different, and the remaining fluid volume and the states are different. Large-pore-fine-throat reservoirs have developed intergranular and dissolution pores, with large effective pore space and high residual movable fluid content. However, the remaining movable fluid is the least in the macro-pore-micro-throat type reservoirs.

#### 4.4 Relationship Between Pore-Throat Heterogeneity at Different Scales and Movable Fluid Saturation

It can be seen from Figure 10 that with the increase of core permeability, the movable oil saturation increases. The change trend of the movable oil controlled by different pore-throat radius is different. When the pore-throat radius is between 0.1 and 0.5  $\mu\text{m}$  and with the peak point of permeability (0.03 and 0.3 mD) as the boundary, there is a good correspondence between the permeability



and the change of movable oil saturation. Especially when the permeability is less than 0.10 mD and greater than 0.3 mD, the movable oil first increases and then decreases with the permeability and pore development degree. When the pore-throat radius is between 0.5 and 1.0  $\mu\text{m}$ , the movable oil saturation first increases and then decreases with the permeability and pore development degree. When the permeability is greater than 0.3 mD and the intergranular and dissolution pores are relatively developed, the movable oil saturation tends to be opposite, with the development degree of pores due to the small throat radius. When the pore-throat radius is greater than 1.0  $\mu\text{m}$ , the combination types of intergranular and dissolution pores develop, and the permeability boundary is 0.3 mD, but the movable oil changes little with the permeability and the degree of pore development. The above analysis shows that the change trend of movable oil is the largest in the range of pore-throat radius of 0.1–0.5  $\mu\text{m}$ ; however, when the permeability is larger and the intergranular pores are developed, the movable oil saturation shows a decreasing trend and fluctuates greatly (Zhang et al., 2006; Zhao et al., 2017; Zhong, 2017).

The relationship between pore-throat uniformity and movable fluid saturation at different scales is shown in Figure 11. It can be seen from Figure 11 that there is a good exponential relationship between the pore-throat heterogeneity of different scales and the movable fluid saturation in the macro-pore-fine-throat, macro-pore-micro-/fine-throat, and macro-pore-micro-throat reservoirs. In the pore-throat range of 0.1–0.5  $\mu\text{m}$ , 0.5–1.0  $\mu\text{m}$ , and greater than 1.0  $\mu\text{m}$ , the greater the uniformity of the pore throat, the greater the saturation of the movable fluids. Intergranular and dissolution pores are mainly developed in the pore-throat interval larger than 1.0  $\mu\text{m}$ , and the relationship between pore-throat uniformity and movable fluid saturation is the best, followed by the 0.1–0.5  $\mu\text{m}$  pore-throat interval. This is mainly because only a small amount of intergranular and dissolution pores are retained in this pore-throat interval, and intercrystalline and micro-pores are mainly developed (Zou et al., 2012; Zhu et al., 2013). In the pore-throat range of 0.5–1.0  $\mu\text{m}$ , the relationship between the pore-throat uniformity and the movable fluid saturation is the worst. This is mainly due to the development of intergranular and dissolution pores, as well as intercrystalline pores and micro-pores.

## 5 CONCLUSION

- (1) The main types of pores developed in the target layer are intergranular pores, followed by feldspar dissolution pores. The radius distribution of the intergranular pores is between 5.0 and 210  $\mu\text{m}$ , with an average value of 50.27  $\mu\text{m}$ . In addition, the pore combination types with the best petrophysical properties are the intergranular pore type, the intergranular-dissolution pore type, and the dissolution-intergranular pore type; their average permeability is 0.62 mD, 0.40 mD, 0.44 mD, and their average porosity is 12.0, 12.3, 12.3%, respectively.
- (2) The target sandstones contain four typical  $T_2$  relaxation time types. The large-pore-fine-throat combination reservoir has the best petrophysical properties. The larger the pore-throat uniformity value, the more uniform the pore-throat radius, and the greater the reservoir permeability. Therefore, the uniformity of throat development controls the seepage capacity of the tight reservoirs.
- (3) The movable fluid saturation of different pore types has obvious differences. The movable fluid saturations at the 0.1 and 0.5  $\mu\text{m}$  pore diameters of the macro-pore-fine-throat and macro-pore-micro-throat reservoirs both show an obvious inflection point, and the movable water saturation is higher with a larger throat radius.

## REFERENCES

- Anovitz, L. M., and Cole, D. R. (2015). 4. Characterization and Analysis of Porosity and Pore Structures. *Rev. Mineral. Geochem.* 80 (1), 61–164. doi:10.1515/9781501502071-004
- Anovitz, L. M., Cole, D. R., Rother, G., Allard, L. F., Jackson, A. J., and Littrell, K. C. (2013). Diagenetic Changes in Macro- to Nano-Scale Porosity in the St. Peter Sandstone: an (Ultra) Small Angle Neutron Scattering and Backscattered Electron Imaging Analysis. *Geochimica Cosmochimica Acta* 102, 280–305. doi:10.1016/j.gca.2012.07.035
- Bukar, M., Worden, R. H., Bukar, S., and Shell, P. (2021). Diagenesis and its Controls on Reservoir Quality of the Tambar Oil Field, Norwegian North Sea. *Energy Geosci.* 2 (1), 10–31. doi:10.1016/j.engeos.2020.07.002
- Cai, M. F. (2020). Key Theories and Technologies for Surrounding Rock Stability and Ground Control in Deep Mining. *J. Min. Strata Control. Eng.* 2 (3), 033037. doi:10.13532/j.jmsce.cn10-1638/td.20200506.001
- Cao, L., Yao, Y., Cui, C., and Sun, Q. (2020). Characteristics of *In-Situ* Stress and its Controls on Coalbed Methane Development in the Southeastern Qinshui Basin, North China. *Energy Geosci.* 1 (1–2), 69–80. doi:10.1016/j.engeos.2020.05.003
- Chen, D., Pang, X., Xiong, L., Wang, L., and Xie, M. (2014). Porosity Evolution in Tight Gas Sands of the Upper Triassic Xujiahe Formation, Western Sichuan Basin, China. *Rev. Mex. Ciencias Geol.* 31, 361–375.
- Desbois, G., Urai, J. L., Kukla, P. A., Konstanty, J., and Baerle, C. (2011). High-resolution 3D Fabric and Porosity Model in a Tight Gas Sandstone Reservoir: A New Approach to Investigate Microstructures from Mm- to Nm-Scale Combining Argon Beam Cross-Sectioning and SEM Imaging. *J. Petroleum Sci. Eng.* 78, 243–257. doi:10.1016/j.petrol.2011.06.004
- Ghanizadeh, A., Clarkson, C. R., Aquino, S., Ardakani, O. H., and Sanei, H. (2015). Petrophysical and Geomechanical Characteristics of Canadian Tight Oil and Liquid-Rich Gas Reservoirs: I. Pore Network and Permeability Characterization. *Fuel* 153, 664–681. doi:10.1016/j.fuel.2015.03.020
- Gier, S., Worden, R. H., Johns, W. D., and Kurzweil, H. (2008). Diagenesis and Reservoir Quality of Miocene Sandstones in the Vienna Basin, Austria. *Mar. Petroleum Geol.* 25 (8), 681–695. doi:10.1016/j.marpetgeo.2008.06.001

## DATA AVAILABILITY STATEMENT

The original contributions presented in the study are included in the article/Supplementary Material; further inquiries can be directed to the corresponding author.

## AUTHOR CONTRIBUTIONS

The first author (QG) is responsible for the technical idea and the remaining authors (MD, HM, and JJ) are responsible for the experimental part of this study.

## FUNDING

This research was supported by the Opening Foundation of State Key Laboratory of Continental Dynamics, Northwest University, “Quantitative characterization and evaluation of micro nano pore structure of tight reservoir based on multifractal theory (No. 21LCD05)” and Doctoral Research Fund of Lanzhou City University, “Study on micro pore structure and seepage mechanism of unconventional tight reservoir in Ordos Basin (No. LZCU-BS2021-01).”

- Hong, D., Cao, J., Wu, T., Dang, S., Hu, W., and Yao, S. (2020). Authigenic Clay Minerals and Calcite Dissolution Influence Reservoir Quality in Tight Sandstones: Insights from the Central Junggar Basin, NW China. *Energy Geosci.* 1 (1–2), 8–19. doi:10.1016/j.engeos.2020.03.001
- Hower, J. C., and Groppo, J. G. (2021). Rare Earth-Bearing Particles in Fly Ash Carbons: Examples from the Combustion of Eastern Kentucky Coals. *Energy Geosci.* 2 (2), 90–98. doi:10.1016/j.engeos.2020.09.003
- Huang, F. R., Yan, S. X., Wang, X. L., Jiang, P. C., and Zhan, S. B. (2021). Experimental Study on Infrared Radiation Characteristics of Gneiss under Uniaxial Compression. *J. Min. Strata Control. Eng.* 3 (1), 013011. doi:10.13532/j.jmsce.cn10-1638/td.20200730.001
- Jiang, T., Zhang, J., and Wu, H. (2017). Effects of Fractures on the Well Production in a Coalbed Methane Reservoir. *Arab. J. Geosci.* 10 (22), 494. doi:10.1007/s12517-017-3283-7
- Kang, H. P. (2021). Temporal Scale Analysis on Coal Mining and Strata Control Technologies. *J. Min. Strata Control. Eng.* 3 (1), 013538. doi:10.13532/j.jmsce.cn10-1638/td.20200814.001
- Kwak, D., Han, S., Han, J., Wang, J., Lee, J., and Lee, Y. (2018). An Experimental Study on the Pore Characteristics Alteration of Carbonate during Waterflooding. *J. Petroleum Sci. Eng.* 161, 349–358. doi:10.1016/j.petrol.2017.11.051
- Lai, J., and Wang, G. (2015). Fractal Analysis of Tight Gas Sandstones Using High-Pressure Mercury Intrusion Techniques. *J. Nat. Gas Sci. Eng.* 24, 185–196. doi:10.1016/j.jngse.2015.03.027
- Lai, J., Wang, G., Wang, S., Cao, J., Li, M., Pang, X., et al. (2018b). Review of Diagenetic Facies in Tight Sandstones: Diagenesis, Diagenetic Minerals, and Prediction via Well Logs. *Earth-Science Rev.* 185, 234–258. doi:10.1016/j.earscirev.2018.06.009
- Lai, J., Wang, G., Wang, Z., Chen, J., Pang, X., Wang, S., et al. (2018a). A Review on Pore Structure Characterization in Tight Sandstones. *Earth-Science Rev.* 177, 436–457. doi:10.1016/j.earscirev.2017.12.003
- Lan, S. R., Song, D. Z., Li, Z. L., and Liu, Y. (2021). Experimental Study on Acoustic Emission Characteristics of Fault Slip Process Based on Damage Factor. *J. Min. Strata Control. Eng.* 3 (3), 023038. doi:10.13532/j.jmsce.cn10-1638/td.20210510.002

- Lei, T., Bikash, K. S., and Michael, S. (2012). Estimation of Horizontal Stress Magnitudes and Stress Coefficients of Velocities Using Borehole Sonic Data. *Geophysics* 77 (3), 181–196. doi:10.1190/geo2011-0277.1
- Li, G., Qin, Y., Shen, J., Wu, M., Li, C., Wei, K., et al. (2019). Geochemical Characteristics of Tight Sandstone Gas and Hydrocarbon Charging History of Linxing Area in Ordos Basin, China. *J. Petroleum Sci. Eng.* 177, 198–207. doi:10.1016/j.petrol.2019.02.023
- Li, H., and Zhang, J. (2011). Elastic Moduli of Dry Rocks Containing Spheroidal Pores Based on Differential Effective Medium Theory. *J. Appl. Geophys.* 75, 671–678. doi:10.1016/j.jappgeo.2011.09.012
- Li, Z., Wu, S., Xia, D., Zhang, X., and Huang, M. (2017). Diagenetic Alterations and Reservoir Heterogeneity within the Depositional Facies: a Case Study from Distributary-Channel Belt Sandstone of Upper Triassic Yanchang Formation Reservoirs (Ordos Basin, China). *Mar. Petroleum Geol.* 86, 950–971. doi:10.1016/j.marpetgeo.2017.07.002
- Liu, J., Zhang, G., Bai, J., Ding, W., Yang, H., and Liu, Y. (2022). Quantitative Prediction of the Drilling Azimuth of Horizontal Wells in Fractured Tight Sandstone Based on Reservoir Geomechanics in the Ordos Basin, Central China. *Mar. Petroleum Geol.* 136, 105439. doi:10.1016/j.marpetgeo.2021.105439
- Liu, Y., Chen, L., Tang, Y., Zhang, X., and Qiu, Z. (2022). Synthesis and Characterization of Nano-SiO<sub>2</sub>@octadecylbisimidazole Quaternary Ammonium Salt Used as Acidizing Corrosion Inhibitor. *Rev. Adv. Mater. Sci.* 61 (1), 186–194. doi:10.1515/rams-2022-0006
- Liu, Y., Gao, M., and Zhao, H. (2020). Detection of Overlying Rock Structure and Identification of Key Stratum by Drilling and Logging Technology. *J. Min. Strata Control Eng.* 2 (2), 81–89. doi:10.13532/j.jmsce.cn10-1638/td.2020.02.004
- Luo, Y., Huang, H., Jakobsen, M., Yang, Y., Zhang, J., and Cai, Y. (2019). Prediction of Porosity and Gas Saturation for Deep-Buried Sandstone Reservoirs from Seismic Data Using an Improved Rock-Physics Model. *Acta Geophys.* 67, 557–575. doi:10.1007/s11600-019-00274-6
- Luo, Y., Huang, H., Yang, Y., Hao, Y., Zhang, S., and Li, Q. (2018). Integrated Prediction of Deepwater Gas Reservoirs Using Bayesian Seismic Inversion and Fluid Mobility Attribute in the South China Sea. *J. Nat. Gas Sci. Eng.* 59, 56–66. doi:10.1016/j.jngse.2018.08.019
- Ma, R. H. (2005). Fracture Prediction of Tight Sandstone Reservoir. *Nat. Gas. Ind.* 25 (10), 36–37.
- Mahmud, H. B., Bin Muhammad Hisham, M. H., Mahmud, W. M., Leong, V. H., and Shafiq, M. U. (2020). Petrophysical Interpretations of Subsurface Stratigraphic Correlations, Baram Delta, Sarawak, Malaysia. *Energy Geosci.* 1 (3–4), 100–114. doi:10.1016/j.engeos.2020.04.005
- Malatesta, C., Federico, L., Crispini, L., and Capponi, G. (2018). Fluid-controlled Deformation in Blueschist-Facies Conditions: Plastic vs Brittle Behaviour in a Brecciated Mylonite (Voltri Massif, Western Alps, Italy). *Geol. Mag.* 155 (2), 335–355. doi:10.1017/s0016756816001163
- Meng, Q., Hooker, J., and Cartwright, J. (2017). Lithological Control on Fracture Cementation in the Keuper Marl (Triassic), North Somerset, UK. *Geol. Mag.* 154, 1–15. doi:10.1017/s001675681700070x
- Mirzaei-Paibaman, A., and Ghanbarian, B. (2021). A New Methodology for Grouping and Averaging Capillary Pressure Curves for Reservoir Models. *Energy Geosci.* 2 (1), 52–62. doi:10.1016/j.engeos.2020.09.001
- Pang, Y.-M., Guo, X.-W., Han, Z.-Z., Zhang, X.-H., Zhu, X.-Q., Hou, F.-H., et al. (2019). Mesozoic-Cenozoic Denudation and Thermal History in the Central Uplift of the South Yellow Sea Basin and the Implications for Hydrocarbon Systems: Constraints from the CSDP-2 Borehole. *Mar. Petroleum Geol.* 99, 355–369. doi:10.1016/j.marpetgeo.2018.10.027
- Qiao, J., Zeng, J., Jiang, S., and Wang, Y. (2020). Impacts of Sedimentology and Diagenesis on Pore Structure and Reservoir Quality in Tight Oil Sandstone Reservoirs: Implications for Macroscopic and Microscopic Heterogeneities. *Mar. Petroleum Geol.* 111, 279–300. doi:10.1016/j.marpetgeo.2019.08.008
- Qie, L., Shi, Y. N., and Liu, J. S. (2021). Experimental Study on Grouting Diffusion of Gangue Solid Filling Bulk Materials. *J. Min. Strata Control Eng.* 3 (2), 023011. doi:10.13532/j.jmsce.cn10-1638/td.20201111.001
- Ren, D., Zhou, D., Liu, D., Dong, F., Ma, S., and Huang, H. (2019). Formation Mechanism of the Upper Triassic Yanchang Formation Tight Sandstone Reservoir in Ordos Basin-Take Chang 6 Reservoir in Jiyuan Oil Field as an Example. *J. Petroleum Sci. Eng.* 178, 497–505. doi:10.1016/j.petrol.2019.03.021
- Rezaee, R., Saeedi, A., and Clennell, B. (2012). Tight Gas Sands Permeability Estimation from Mercury Injection Capillary Pressure and Nuclear Magnetic Resonance Data. *J. Petroleum Sci. Eng.* 88–89, 92–99. doi:10.1016/j.petrol.2011.12.014
- Saeini, A., and Riahi, Z. (2017). Controls on Fracture Distribution in Cretaceous Sedimentary Rocks from the Isfahan Region, Iran. *Geol. Mag.* 154, 1–13. doi:10.1017/s0016756817000346
- Santosh, M., and Feng, Z. Q. (2020). New Horizons in Energy Geoscience. *Energy Geosci.* 1 (1–2), A1. doi:10.1016/j.engeos.2020.05.005
- Sebacher, B., Hanea, R., and Stordal, A. S. (2017). An Adaptive Pluri-Gaussian Simulation Model for Geological Uncertainty Quantification. *J. Petroleum Sci. Eng.* 158, 494–508. doi:10.1016/j.petrol.2017.08.038
- Shanley, K. W., and Cluff, R. M. (2015). The Evolution of Pore-Scale Fluid-Saturation in Low-Permeability Sandstone Reservoirs. *Bulletin* 99, 1957–1990. doi:10.1306/03041411168
- Shi, B., Chang, X., Yin, W., Li, Y., and Mao, L. (2019). Quantitative Evaluation Model for Tight Sandstone Reservoirs Based on Statistical Methods - A Case Study of the Triassic Chang 8 Tight Sandstones, Zhenjing Area, Ordos Basin, China. *J. Petroleum Sci. Eng.* 173, 601–616. doi:10.1016/j.petrol.2018.10.035
- Sun, W., Li, Y. F., Fu, J. W., and Li, T. Y. (2014). Review of Fracture Identification with Well Logs and Seismic Data. *Prog. Geophys.* 29 (3), 1231–1242. doi:10.6038/pg20140332
- Wang, A., Zhong, D., Zhu, H., Guo, L., Li, Z., Jiang, Y., et al. (2018a). Depositional and Diagenetic Controls on the Reservoir Quality of Upper Triassic Chang-7 Tight Oil Sandstones, Southwestern Ordos Basin, China. *Geosci. J.* 23 (3), 471–488. doi:10.1007/s12303-018-0042-z
- Wang, D. L., Hao, B. Y., and Liang, X. M. (2021). Slurry Diffusion of Singlefracture Based on Fluid-Solid Coupling. *J. Min. Strata Control Eng.* 3 (1), 013038. doi:10.13532/j.jmsce.cn10-1638/td.20200429.001
- Wang, L., Zhao, N., Sima, L., Meng, F., and Guo, Y. (2018b). Pore Structure Characterization of the Tight Reservoir: Systematic Integration of Mercury Injection and Nuclear Magnetic Resonance. *Energy Fuels.* 32 (7), 7471–7484. doi:10.1021/acs.energyfuels.8b01369
- Xi, K., Cao, Y., Haile, B. G., Zhu, R., Jahren, J., Bjørlykke, K., et al. (2016). How Does the Pore-Throat Size Control the Reservoir Quality and Oiliness of Tight Sandstones? the Case of the Lower Cretaceous Quantou Formation in the Southern Songliao Basin, China. *Mar. Petroleum Geol.* 76, 1–15. doi:10.1016/j.marpetgeo.2016.05.001
- Xue, F., Liu, X. X., and Wang, T. Z. (2021). Research on Anchoring Effect of Jointed Rock Mass Based on 3D Printing and Digital Speckle Technology. *J. Min. Strata Control Eng.* 3 (2), 023013. doi:10.13532/j.jmsce.cn10-1638/td.20201020.001
- Yang, J. X., Luo, M. K., Zhang, X. W., Huang, N., and Hou, S. J. (2021). Mechanical Properties and Fatigue Damage Evolution of Granite under Cyclic Loading and Unloading Conditions. *J. Min. Strata Control Eng.* 3 (3), 033016. doi:10.13532/j.jmsce.cn10-1638/td.20210510.001
- Yin, S., Lv, D., and Ding, W. (2018). New Method for Assessing Microfracture Stress Sensitivity in Tight Sandstone Reservoirs Based on Acoustic Experiments. *Int. J. Geomechanics* 18 (4), 1–11. doi:10.1061/(ASCE)GM.1943-5622.0001100
- Yin, S., and Wu, Z. (2020). Geomechanical Simulation of Low-Order Fracture of Tight Sandstone. *Mar. Petroleum Geol.* 117, 1–10. doi:10.1016/j.marpetgeo.2020.104359
- Yoshida, M., and Santosh, M. (2020). Energetics of the Solid Earth: An Integrated Perspective. *Energy Geosci.* 1 (1–2), 28–35. doi:10.1016/j.engeos.2020.04.001
- Zhang, B., Shen, B., and Zhang, J. (2020). Experimental Study of Edge-Opened Cracks Propagation in Rock-like Materials. *J. Min. Strata Control Eng.* 2 (3), 033035. doi:10.13532/j.jmsce.cn10-1638/td.20200313.001
- Zhang, J., Ju, Y., and Zhang, Q. (2019). Low Ecological Environment Damage Technology and Method in Coal Mines. *J. Min. Strata Control Eng.* 1 (1), 013515. doi:10.13532/j.jmsce.cn10-1638/td.2019.02.005
- Zhang, T., Switzer, P., and Journel, A. (2006). Filter-Based Classification of Training Image Patterns for Spatial Simulation. *Math. Geol.* 38 (1), 63–80. doi:10.1007/s11004-005-9004-x
- Zhao, H., Ning, Z., Wang, Q., Zhang, R., Zhao, T., Niu, T., et al. (2015). Petrophysical Characterization of Tight Oil Reservoirs Using Pressure-Controlled Porosimetry Combined with Rate-Controlled Porosimetry. *Fuel* 154, 233–242. doi:10.1016/j.fuel.2015.03.085
- Zhao, J. L., Liu, J. J., Zhang, Q. H., and Qu, X. R. (2017). Overview of Geophysical Exploration Methods and Technical of Tight Sandstone Gas Reservoirs. *Prog. Geophys.* 32 (2), 840–848. doi:10.6038/pg20170253
- Zhong, D. (2017). Micro-petrology, Pore Throat Characteristics and Genetic Mechanism of Tight Oil Reservoirs - A Case from the 6th and 7th

- Members of Triassic Yanchang Formation in the Ordos Basin. *Oil Gas Geol.* 38 (1), 49–61. doi:10.11743/ogg20170106
- Zhou, N., Lu, S., Wang, M., Huang, W., Xiao, D., Jiao, C., et al. (2021). Limits and Grading Evaluation Criteria of Tight Oil Reservoirs in Typical Continental Basins of China. *Petroleum Explor. Dev.* 48 (5), 1089–1100. doi:10.1016/S1876-3804(21)60093-9
- Zhu, R., Bai, B., Cui, J., Wang, T., Niu, L., and Li, T. (2013). Research Advances of Microstructure in Unconventional Tight Oil and Gas Reservoirs. *J. Palaeogeogr.* 15, 615–623.
- Zou, C., Zhu, R., Liu, K., Su, L., Bai, B., Zhang, X., et al. (2012). Tight Gas Sandstone Reservoirs in China: Characteristics and Recognition Criteria. *J. Petroleum Sci. Eng.* 88–89, 82–91. doi:10.1016/j.petrol.2012.02.001

**Conflict of Interest:** MD was employed by the Fuxian Oil Production Plant, Yanchang Petroleum (Group).Ltd., HM was employed by the Oil Production Plant, Changqing Oilfield Company, and JJ was employed by the Oil Production Plant, Changqing Oilfield Company.

The remaining authors declare that the research was conducted in the absence of any commercial or financial relationships that could be construed as a potential conflict of interest.

**Publisher's Note:** All claims expressed in this article are solely those of the authors and do not necessarily represent those of their affiliated organizations, or those of the publisher, the editors and the reviewers. Any product that may be evaluated in this article, or claim that may be made by its manufacturer, is not guaranteed or endorsed by the publisher.

Copyright © 2022 Guo, Dong, Mao and Ju. This is an open-access article distributed under the terms of the Creative Commons Attribution License (CC BY). The use, distribution or reproduction in other forums is permitted, provided the original author(s) and the copyright owner(s) are credited and that the original publication in this journal is cited, in accordance with accepted academic practice. No use, distribution or reproduction is permitted which does not comply with these terms.